Iron oxidation state in garnet from a subduction setting: a micro-XANES and electron microprobe ("flank method") comparative study

Iron oxidation state in garnet from a subduction setting: a micro-XANES and electron microprobe ("flank method") comparative study

Elisa Borfecchia, Lorenzo Mino, Diego Gianolio, Chiara Groppo, Nadia Malaspina, Gema Martinez-Criado, Juan Angel Sans Tresserras, Stefano Poli, Daniele Castelli and Carlo Lamberti

J. Anal. At. Spectrom., **2012**, *27*, 1725–1733

DOI: 10.1039/c2ja30149k

Iron oxidation state in garnet from a subduction setting: a micro-XANES and electron microprobe ("flank method") comparative study

Elisa Borfecchia[a], Lorenzo Mino[a*], Diego Gianolio[a], Chiara Groppo[b*], Nadia Malaspina[c], Gema Martinez-Criado[d], Juan Angel Sans Tresserras[d], Stefano Poli[e], Daniele Castelli[b] and Carlo Lamberti[a]

The variation of the Fe-redox state across a strongly zoned garnet crystal occurring in a FeTi-oxide metagabbro from a subduction setting has been investigated comparing micro-XANES and electron microprobe ("flank method") results. This sample represents an ideal monitor of the redox processes associated to devolatilization reactions occurring in the subducting slab and likely involved in the oxidation of the mantle wedge, as well as a challenge for the analytical methods. Since in the studied garnet the $Fe^{3+}/\Sigma Fe$ variations are small and occur on a micrometric scale, we exploited the X-ray microprobe available at the ESRF ID22 beamline to reach a spot size of 1.7 μm × 5.3 μm. Our study represents a first attempt to measure the $Fe^{3+}/\Sigma Fe$ variations across a single crystal of garnet, ca. 400 μm in diameter, using the micro-XANES technique. The absolute $Fe^{3+}/\Sigma Fe$ values obtained with micro-XANES and "flank method" are perfectly comparable, ranging from a maximum of about 0.1 in the garnet core to a minimum of 0.0 in the garnet rim.

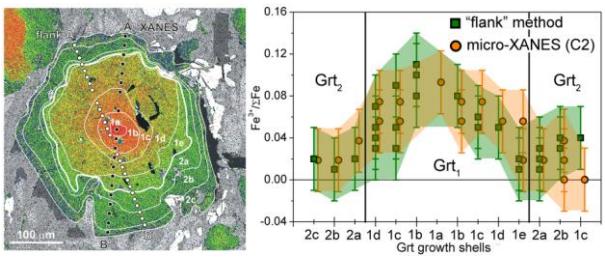

The comparison of micro-XANES and "flank method" results allowed us to fully explore on the micrometric scale the $Fe^{3+}/\Sigma Fe$ variations in a strongly zoned garnet crystal from a subduction setting

1 Introduction

Detailed studies of devolatilization reactions and metamorphic transformations occurring in the subducting slab play a key role in unravelling the complex physical-chemical transformation of crust and mantle at convergent margins. Fluids released from the subducting slab are, in fact, considered as the primary source of volatiles for arc magmatism and fluid-induced seismicity.[1,2] The volatile transfer from the slab to the mantle wedge is also considered as responsible for the higher oxygen fugacity recorded by the mantle wedge with respect to the subcratonic lithospheric mantle that equilibrated at similar pressures.[1,3-6] Although it is accepted that the mantle wedge above subduction zones is oxidized, the exact processes of relative oxidation are still controversial.[1,7,8] The study of the redox reactions occurring at the interface between the subducting slab and the mantle wedge, in fact, is hampered by the difficulties in accurately determining the oxidation state of the involved phase assemblages. In particular, micro-scale measurements of $Fe^{3+}/\Sigma Fe$ ratio are sorely needed to enable us to begin to understand variations in redox conditions during subduction.

Standard electron microprobe (EMP) analyses are not able to discriminate between oxidation state of Fe, and the $Fe^{3+}/\Sigma Fe$ ratio is generally calculated by charge balance methods,[9] whose reliability, however, depends on the accuracy of the specific EMP analysis. It has been demonstrated that this method often fails in determining the correct $Fe^{3+}/\Sigma Fe$ ratio.[10-12] On the other hand, bulk methods like wet chemistry[13] or conventional Mössbauer spectroscopy lack information on mineral zoning and variance from different textural positions of the mineral phases. Recent advances in spectroscopic and microprobe techniques (i.e. micro-Mössbauer[14,15] and electron microprobe "flank method"[16]) are opening new possibilities for the determination of redox state in Fe-bearing minerals.[5,6] The analytical methods currently available for the determination of $Fe^{3+}/\Sigma Fe$ ratio in garnets will be briefly reviewed in Section 2.

In particular, micro-XANES spectroscopy is an appropriate method for the space-resolved determination of ferric iron contents on micrometric crystals without destroying their textural context.[17-20] This technique has advantages over Mössbauer spectroscopy relating to superior spatial resolution and significantly shorter data acquisition times.[20-22] However, most of the studies conducted so far on garnets were aimed to the calibration of the XANES technique and were performed on powdered samples, natural or synthetic, with known $Fe^{3+}/\Sigma Fe$ ratios.[22,23] Powdered samples can be assumed to be homogeneous, this means that the problem of spatial resolution is overcome. Micro-XANES technique has been applied on garnet single crystals (thin sections) in few studies[18,20,24] and chemical variations across single crystals were not investigated in details (i.e. chemical profiles from core to rim were not performed).

In this paper we report the results of a comparative micro-XANES and electron microprobe "flank method" study on strongly-zoned garnet single crystals (ca. 400 μm in diameter) from an eclogitic FeTi-oxide gabbro (Monviso meta-ophiolites, western Alps), aimed to the determination of the $Fe^{3+}/\Sigma Fe$ variation across the crystals. The studied sample, which extraordinarily well preserves evidence of its prograde evolution during subduction down to a depth of ca. 80 km (Fig. 1), has been already fully characterized on the petrological ground.[25] This sample represents an ideal monitor of the redox processes associated to devolatilization reactions occurring in the subducting slab and likely involved in the oxidation of the mantle wedge.

The challenge of our study was twofold: (i) the spatial resolution must be of the order of microns, because we expected that $Fe^{3+}/\Sigma Fe$ variations occur on a micrometric scale; (ii) the $Fe^{3+}/\Sigma Fe$ variations across the garnet crystal are small, therefore the spectral resolution must be as small as possible in order to appreciate the differences in the oxidation state of garnet.

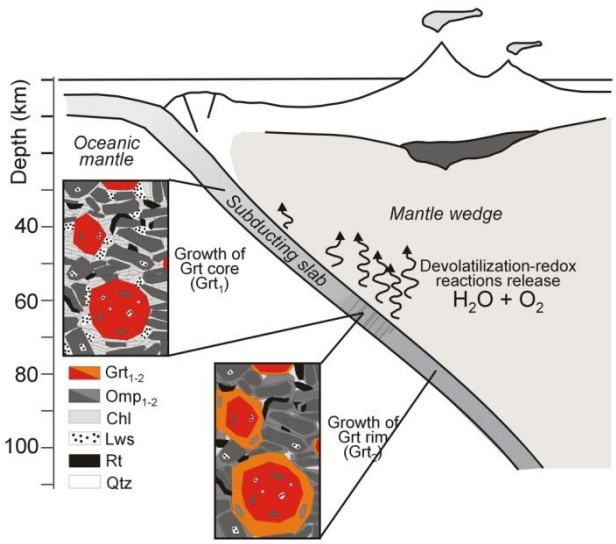

Fig.1 Sketch of the subduction setting relevant to this study. The progressively darker grey colour of the subducting oceanic crust implies higher density balanced by lower H_2O content. The darker dashed field along the subducting slab approximates the lawsonite and chlorite breakdown, corresponding to a depth at which the maximum H_2O and O_2 are released from the eclogite into the mantle wedge (see Groppo and Castelli, 2010[25] for further details). Mantle wedge (light grey) is more oxidized then oceanic mantle (white). The two boxes depict two different stages in the prograde evolution of the studied sample OF2727, including the growth of core and rim garnet (Grt_1 and Grt_2, respectively). Abbreviations: Grt = garnet; Omp = omphacite; Chl = chlorite; Lws = lawsonite; Rt = rutile; Qtz = quartz.

2. Analytical methods for the determination of $Fe^{3+}/\Sigma Fe$ ratio in garnet: state of the art

Different methods are actually available to determine the $Fe^{3+}/\Sigma Fe$ ratio in silicate phases, and in particular, in garnets. The traditional bulk methods, such as chemical titration and the traditional Mössbauer spectroscopy, require the dissolution or grinding of the sample and thus lacking information on mineral zoning and variance from different textural positions. The most suitable techniques used so far for measuring the $Fe^{3+}/\Sigma Fe$ ratio in garnets at micro- to nano-metric scale are: the micro-Mössbauer spectroscopy, the electron energy loss spectroscopy (EELS), the "flank method" performed on wavelength-dispersive spectra using an electron microprobe, and the micro-X-ray absorption near edge structure (micro-XANES) spectroscopy.

2.1 Micro-Mössbauer Spectroscopy

Strongly-zoned mantle garnets from metasomatized peridotitic xenoliths were analysed by McCammon *et al.*[15] using Mössbauer spectroscopy with a high spatial resolution of 400 μm. High quality Mössbauer spectra can be, however, recorded on diameters as small as 50 μm. The obtained Mössbauer spectra revealed a significant increase in $Fe^{3+}/\Sigma Fe$ from garnet core to garnet rim (from 0.05 to 0.10), thus suggesting a change in the redox conditions at different stages of garnet growth. The spectra were recorded at room temperature in transmission mode, over a time period ranging from 1 – 5 days depending on the signal quality. Errors in the $Fe^{3+}/\Sigma Fe$ ratio with micro-Mössbauer technique are usually estimated to be on the order of ± 0.02 – 0.03.[15]

2.2 Electron Energy Loss Spectroscopy (EELS)

The EELS technique, which combines electron energy-loss spectroscopy and transmission electron microscopy,[26] allows the quantitative determination of the ferric iron concentration in minerals with high spatial resolution on a scale down to 10 nm. The acquisition time is considerably less than that required by micro-Mössbauer spectroscopy (15 – 30 s for each spectra), thus allowing the possibility of analysing large number of samples or $Fe^{3+}/\Sigma Fe$ profiles. As concerning garnets, van Aken *et al.*[27] applied this technique on synthetic and natural mantle garnets and proposed well calibrated white line intensities of the Fe L_{23} edges. Malaspina *et al.*[6] used the EELS technique to measure the $Fe^{3+}/\Sigma Fe$ ratio of pyrope-rich garnets from orogenic mantle peridotites (Sulu UHP belt, China). The obtained spectra showed a core-to-rim zoning with decreasing $Fe^{3+}/\Sigma Fe$ ratio toward the rim. Errors in the $Fe^{3+}/\Sigma Fe$ ratio with EELS are usually estimated to be on the order of ±0.05.[27,28]

2.3 Flank Method

The "flank method" allows the determination of the oxidation state of Fe in minerals using the electron microprobe, with the possibility to analyze simultaneously the major element chemistry on the same spot, at a spatial resolution of about 1 μm and with an acquisition time of ca. 300 s.[16,29] The method exploits the behavior of the low-energy emission lines (Lβ and Lα) of iron, which shift with changes of the iron oxidation state. With the "flank method" the Lβ/Lα intensity ratios are measured in correspondence of those Lβ and Lα wavelength positions where the differences between the spectra of pure ferric and ferrous iron-bearing samples are most pronounced.[29] The "flank method" was developed for garnets by Höfer and Brey[29] using well-characterized synthetic samples, and it was employed by Malaspina *et al.*[5] on natural and synthetic garnet end members with fixed $Fe^{3+}/\Sigma Fe$. Comparisons with data obtained using both Mössbauer spectroscopy and EELS technique on the same samples[6,29,30] yielded excellent agreement between the three techniques, thus demonstrating the accuracy of the "flank method". An error between ± 0.02 and ± 0.04 for $Fe^{3+}/\Sigma Fe$ ratio

has been documented in samples with 8 – 11 wt% total Fe.[29]

2.4 Micro-X-Ray Absorption Near Edge Structure (Micro-XANES) Spectroscopy

The XANES spectroscopy is usually adopted to determine the coordination and oxidation states of transition metal elements in materials[23,31-35] and when a combination of different oxidation states is present, to determine their relative fraction.[36-44] In particular XANES currently allows measurement of the $Fe^{3+}/\Sigma Fe$ ratio in minerals[17,18,20,22-24,45] with a spatial resolution of few microns and an acquisition time of 20 – 30 min, thanks to the micron- and sub-micron X-ray beams available in some dedicated beamlines of third generation synchrotron radiation facilities.[46-53] XANES calibrations on garnet were generally performed on powdered samples,[22,23] whereas so far only few studies have applied the micro-XANES technique for measuring the $Fe^{3+}/\Sigma Fe$ on single garnet crystals at the micrometric scale.[18,20,24] Very low $Fe^{3+}/\Sigma Fe$ ratios were estimated by Dyar *et al.*[24] in garnets from low- to medium-grade metapelites and by Schmid *et al.*[18]in garnets from an eclogite. Errors of ± 0.05 – ±0.15 in the estimate of $Fe^{3+}/\Sigma Fe$ are reported for anisotropic materials,[24] but they can be of about ±0.07 for isotropic crystals, such as garnet.[22,23]

Finally, it is worth noting that all the techniques discussed above have been mostly applied to investigate the $Fe^{3+}/\Sigma Fe$ ratio of garnets from mantle settings (generally characterized by relatively low ΣFe contents), whereas very few data are actually available for the Fe-richer garnets from subduction environments.[18]

All the studies reported above exploit the K absorption edge which is by far the most investigated in the geological field. A possible alternative would be the analysis of Fe L-edges (located in the 700-850 eV range), which can be potentially even more informative owing to the longer core hole lifetime and thus intrinsic narrower energy features. Moreover being L-edges closer than the K-one to the valence levels, they are more affected by a change in the Fe oxidation state.[54-56] Finally, the spatial resolution achievable in the soft X-ray region can be as low as 20 nm. However in this case following issues have to be considered : i) In the soft X-ray domain, the highest spatial resolution is obtained employing Fresnel zone-plate that are chromatic devices whose focal distances change with the photon energy.[53] This means that, in absence of complex energy-dependent sample repositioning the different points of a XANES spectrum will be characterized by a different spatial resolution. ii) In the soft energy region ultrahigh vacuum conditions and thin beryllium windows are required in order to avoid air absorption (the X-ray absorption length in air increases from 900 μm to 0.5 m moving from 700 to 7000 eV). iii) In the range between 100 and 1500 eV the number of available beamlines with suitable XAS set-up is relatively limited. iv) The higher penetration depths of hard X-rays allows investigation of thicker samples without complex sample preparation procedures or without being limited to a sampling of the uppermost layers. v) Hard X-rays provide suitable wavelengths for simultaneous XRD and XRF data acquisitions, which in many cases can provide useful complementary information.

From these considerations, it emerges that in case of thick samples characterized also by a vertical gradient of the oxidation state, the combined use of flank, soft and hard X-rays can represent a non destructive approach to the problem.

3 Experimental

3.1 Samples Description

The studied sample OF2727 is a fine-grained eclogite from the Monviso meta-ophiolite (western Alps), consisting of omphacite, garnet and rutile with minor blue amphibole and very minor lawsonite, talc and jadeite,[57] petrologically interpreted by Groppo and Castelli[25] (see also Fig. 1). The polished thin section (ca. 30 μm thick) is mounted on a high chemical purity SiO_2 amorphous slide using Fe-free Araldit®-epoxy. Garnet occurs as small idioblasts (up to 0.5 mm in diameter) set in a matrix mainly consisting of omphacite. Garnet cores (Grt_1 in Fig. 2a) are crowded of very small inclusions mostly of omphacite, whereas garnet rims (Grt_2 in Fig. 2a) are almost free of inclusions. Both SEM-EDS and EMP analytical techniques have been used to analyze the major element concentrations across garnet crystals. Garnet is strongly zoned, showing a Mn and Ca decrease toward the rim, counterbalanced by a Fe and Mg increase (Fig. 2b). More in detail, the X_{Mn} decreases from 0.24 in the core to 0.00 in the rim and it is balanced by an increase in both X_{Mg} and X_{Fe} (X_{Mg} is 0.01 to 0.12, and X_{Fe} is 0.56 to 0.82 from core to rim, respectively). Ca zoning is more complex, slightly increasing from the inner core to the outer core and decreasing toward the rim (X_{Ca} varies from 0.21 to 0.27 and to 0.11 toward the rim[25]) [X_{Mn} = Mn/(Ca+Mg+Fe^{2+}+Mn); X_{Mg} = Mg/(Ca+Mg+Fe^{2+}+Mn); X_{Ca} = Ca/(Ca+Mg+Fe^{2+}+Mn); X_{Fe} = Fe^{2+}/(Ca+Mg+Fe^{2+}+Mn)].

Two garnet crystals have been analyzed using the "flank method" in order to measure their $Fe^{3+}/\Sigma Fe$ ratio.[25] One of these garnet crystals (in the following referred to as Grt) has been chosen for the micro-XANES study, because microprobe data and X-ray maps showed that compositional variations between core and rim are the maximum allowed (i.e. garnet has been sectioned through the real core). The thin section was carbon coated for the microprobe and "flank method" analyses.

For the calibration (C1) of XANES spectra, almandine ($Fe^{3+}/\Sigma Fe$ = 0), hematite ($Fe^{3+}/\Sigma Fe$ = 1) and magnetite ($Fe^{3+}/\Sigma Fe$ = 2/3) crystals were used as standards. These are high purity reference standards for X-ray microanalysis (SPI Supplies – reference numbers: #AS1020-AB, #AS1180-AB, #AS1210-AB), mounted in a 25 mm diameter, 6 mm thick non-magnetic stainless steel disc.

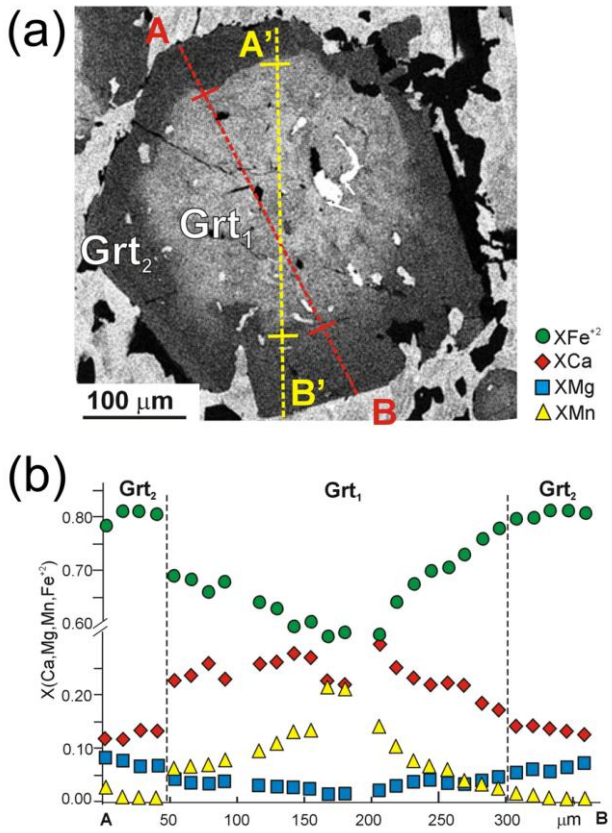

Fig.2 X-ray map for Ca (a) and EMPA compositional profile (b) of the studied garnet crystal. In the map, lighter grey implies higher concentration, as also shown by quantitative spot analyses; the dashed lines A-B and A'-B' locate the two sections analysed using the EMPA-"flank method" and the micro-XANES technique, respectively. The boundary between garnet core (Grt_1) and garnet rim (Grt_2) is outlined in both the X-ray map and compositional profile.

3.2 Micro-XANES Spectroscopy

3.2.1 Beamline Description

Fe K-edge XANES spectra were recorded at the ID22 beamline of the ESRF at Grenoble,[58,59] based on crossed mirrors in Kirkpatrick-Baez (KB) configuration[60] to reach a beam size of 1.7 μm (vertical) × 5.3 μm (horizontal). The basic beamline set-up is reported in Fig. 3.

ID22 is installed on a high-β straight section of the ring equipped with two different undulators: a standard linear undulator (U42 with minimum gap of 16 mm), covering the energy range from 6 to 50 keV, and a second one, which is a so-called in-vacuum linear undulator (U23 with minimum gap of 6 mm). After the front-end, the beam passes through the optics hutch (see Fig. 3a), where a set of selectable high-power filters and slits with adjustable horizontal and vertical apertures optimize the intensity and the shape of the beam. A flat horizontally deflecting Si mirror also allows thermal load reduction and higher harmonic rejection. Then, a Kohzu fixed-exit double crystal monochromator is used with two different pairs of crystals: Si(111) for the low energy range (4 – 33 keV) and Si(311) for higher energies (7 – 72 keV). The latter was used in this work to ensure a better energy resolution.

As shown in Fig. 3b, the microprobe set-up consists of two metallic coated orthogonal reflecting Si mirrors with elliptical shapes which are situated at 41 m from the source on a granite table. Using Au knife-edge scans, a beam size of 1.7 μm (vertical) × 5.3 μm (horizontal) has been determined. Since the efficiency of the KB mirrors reaches approximately 70% using both undulators, the photon flux in the focal spot is about 10^{12} photon/s at 13 keV in uniform filling mode (current in the ESRF ring ~ 200 mA). Two ionization chambers were used to monitor the intensity of the incoming (I_0) and transmitted (I_t) beams. The fluorescence signal coming from the sample was collected with a silicon drift detector (see Fig. 3). A visible light video-microscope allows visualization of the sample for precise alignment in the micro-beam.

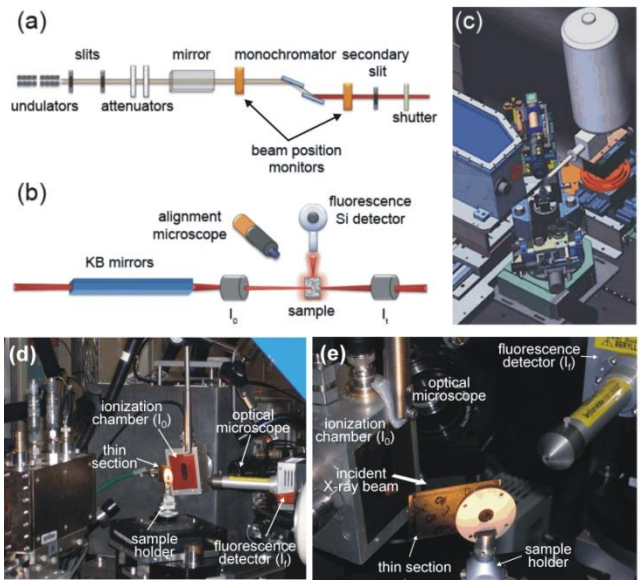

Fig. 3 Experimental set-up used at ESRF ID22 beamline. (a) Scheme of the optic hutch, where the X-rays emitted by U42 and U23 undulators are monochromatized using two Si(311) reflections. (b) Scheme of the experimental hutch, containing the KB focusing mirrors, two ionization chambers to measure I_0 and I_t, the rotating sample holder, the optical microscope for sample/beam alignment, the fluorescence detector. (c) 3-D scheme of the experimental set-up reported in (b). (d, e) Experimental set-up showing the position of the sample.

3.2.2 XANES Acquisition

All XANES spectra were recorded in fluorescence mode. The samples were mounted at 45° with respect to both the incident beam and the Si(Li) solid state fluorescence detector. XANES spectra were recorded using a 2 eV step size for the far pre-edge region and a 0.1 eV step size in the pre-edge and edge regions (7105 – 7135 eV); in the post-edge region (from k = 1.6 $Å^{-1}$ to k = 10 $Å^{-1}$) a k-step of 0.05 $Å^{-1}$ was used. An integration time of 1 second per point was adopted in the whole range except for the region containing the features of interest (7111 – 7119 eV), where the integration time was increased to 5 seconds. The total scan time was 25 – 30 min. A precise calibration of the monochromator energy was carried out by measuring a reference XANES spectrum of a Fe foil (EXAFS Materials Inc.) in transmission geometry and then defining the first derivative peak at the tabulated value of 7112.0 eV.[61] In order to precisely locate the microstructural sites of interest, different μ-XRF profiles were acquired on the garnet crystal. Basing on these compositional

profiles, 22 μ-XANES spectra were acquired along a rim-core-rim profile of Grt (line A'-B' in Fig. 2a), at a distance of 15.3 μm from each other.

The Athena software[62] was used for the extraction of the data. The edge jump was estimated fitting the far pre-edge region (E < 7105 eV) with a linear function, while the post edge was reproduced with a second order spline. Spectra were compared after normalization. Two XANES spectra from the core of Grt were rejected because they were acquired too close to omphacite inclusions.

3.3 Flank Method

The $Fe^{3+}/\Sigma Fe$ ratio of garnet was measured by electron microprobe using the "flank method"[16,29] calibrated on the JEOL 8200 Superprobe at the Department of Earth Sciences, University of Milano.[5] The spectrometer calibration was carried out searching the peak for FeKα (9^{th} order) on a metallic iron standard at 25 kV accelerating voltage and 80 nA beam current using a TAP crystal and the integral pulse height analysis mode. With respect to the Lβ and Lα peaks, the shape of FeKα (9^{th} order) is very sharp, enabling an accurate spectrometer shift correction. Combined "flank method" and quantitative elemental analysis were performed on wavelength-dispersive spectra at 15 kV and 60 nA. One spectrometer with a TAP crystal and 300 μm slit was used for the "flank method", measuring the FeLα and FeLβ at a counting time of 300 s. With the remaining four spectrometers Si, Ti, Al, Cr, Fe, Mg, Mn and Ca were measured simultaneously. Natural silicates were used as standards to measure: Mg, Al, and Si on pyrope, Fe on almandine, Ca on grossular, Mn on rodonite, Cr on chromite, Ti on ilmenite. A PhiRhoZ routine was used for matrix correction.

The quantitative $Fe^{3+}/\Sigma Fe$ in garnets was determined by applying the correction for self-absorption,[29] using natural and synthetic garnet end-members with fixed $Fe^{3+}/\Sigma Fe$ as standards.[5] Mineral analyses were always performed using detailed backscattered electron images to check the microtextural site. 29 analysis were acquired along a rim-core-rim profile of Grt (line A-B in Fig. 2a), at a distance of 13.2 μm from each other. The $Fe^{3+}/\Sigma Fe$ error is between ±0.01 and ±0.03 for our garnets with 21-29 wt% of ΣFe.

4 Results and Discussion

4.1 Micro-XANES Spectroscopy

In a systematic investigation of mantle garnets, the pre-edge energy, which is commonly used for quantification of $Fe^{3+}/\Sigma Fe$,[18,19,21,23,45] was found to be relatively insensitive for synthetic garnets,[22] particularly at low values of $Fe^{3+}/\Sigma Fe$ as expected in our sample. Berry *et al.*[22] concluded that monitoring the absorption edge energy position is a more effective way to extract the $Fe^{3+}/\Sigma Fe$ ratio from garnets. In particular they proposed an empirical correlation between the $Fe^{3+}/\Sigma Fe$ ratio and the energy position of the point closest to the 0.9 value of normalized intensity (in the following referred to as $E_{0.9}$). Therefore, we applied both the approaches (i.e. pre-edge vs. $E_{0.9}$ analysis) to test the feasibility of their application to our natural garnet sample. The same approach is found in the literature for the speciation of the relative amount of different oxidation states for other transition metals such as Cu^{2+}/Cu^{+}[42,43] or Co^{3+}/Co^{4+}.[40] In order to isolate the pre-edge peaks, a background (calculated by modeling the edge jump as the sum of a constant function with an arctangent function: red curve in Fig. 4) was subtracted from the experimental data. The pre-edge features were fitted with three Gaussian functions (Fig. 4c) and the centroid was calculated as the intensity-weighted average energy position of the maxima.

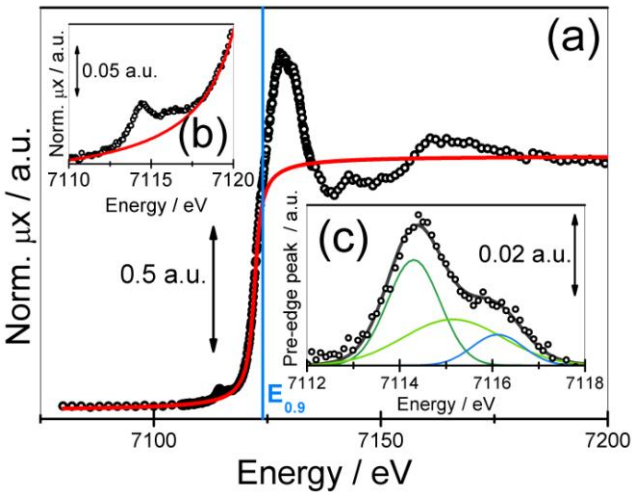

Fig. 4 Example of Fe K-edge μ-XANES spectrum collected on Grt. (a) XANES spectrum acquired at point 7 along the A'-B' line of Fig. 2a (see also Table 1). The simulated background is plotted as a red line; the $E_{0.9}$ position is indicated by the blue line. (b) Enlarged detail of (a) in the pre-edge region. (c) Deconvolution of pre-edge features using three Gaussian functions after background subtraction.

Analyzing the energy positions of the pre-edge centroids reported in Table 1, we can conclude that it is not possible to identify clear differences in the centroid positions along the Grt profile. Therefore, our μ-XANES analysis confirms what was previously suggested for synthetic garnets,[22] i.e. the relative insensitivity of the pre-edge centroid position to small variations in the $Fe^{3+}/\Sigma Fe$ ratio.

The second approach tested was based on the determination of $E_{0.9}$. As visible from Table 1, the $E_{0.9}$ values obtained for different positions along the Grt profile are significantly different, thus confirming the effectiveness of the $E_{0.9}$ approach also in natural garnets.

In order to quantify the $Fe^{3+}/\Sigma Fe$ ratio variation along our sample, a crucial issue is represented by the reference minerals selected for the calibration procedure. It is well known that, due to matrix effects, the quantitative estimate of $Fe^{3+}/\Sigma Fe$ in garnet requires the use of a large set of standards, with compositions similar to the composition of the investigated sample.[22] However, such well characterized garnet standards are generally not easily available, thus hampering the routinary application of the micro-XANES technique for petrological purposes. For this reason, we have initially used three standards (almandine, magnetite and hematite) commonly supplied to the EMP laboratories. These standards have the additional advantage of being themselves single crystals (ca. 30 μm thick) as the studied garnet. A calibration line (C1) was thus calculated fitting the known $Fe^{3+}/\Sigma Fe$ ratio of almandine, hematite and magnetite as a function of $E_{0.9}$ (dark grey dashed line in Fig. 5). The goodness of the fit was checked using its standard deviation σ_f defined as:

$$\sigma_f = \sqrt{\frac{\sum_{i=1}^{N}(y_{exp,i} - y_{fit,i})^2}{N-2}} \quad (1)$$

where $y_{exp,i}$ is the ordinate of the *i*th experimental point (in our case the $Fe^{3+}/\Sigma Fe$ value), $y_{fit,i}$ is the ordinate corresponding to the abscissa $x_{exp,i}$ on the best fit line and N is the number of experimental points. Owing to the limited number of references minerals included in the C1 calibration, a rather large standard deviation ($\sigma_f = 0.103$) was obtained.

In order to overcome this limitation, an alternative calibration line has been obtained by exploiting literature data on a complete set of synthetic Fe^{+3}-bearing garnets.[22] The linear fit (C2) performed in this way (red dashed line in Fig. 5) shows a much better value of standard deviation ($\sigma_f = 0.029$).

The $Fe^{3+}/\Sigma Fe$ ratios obtained using the two calibrations are reported in Table 1: they decrease from a maximum of 0.14 in the garnet core to a minimum of 0.00 in the rim in the case of calibration C1, while they vary in the 0.00 – 0.09 interval for calibration C2.

Table 1 Energy positions of the pre-edge centroids and $E_{0.9}$, and corresponding calculated $Fe^{3+}/\Sigma Fe$ ratios for the micro-XANES spectra acquired on Grt

Sample	Pre-edge Centroid (eV)	$E_{0.9}$ (eV)	$Fe^{3+}/\Sigma Fe$ C1	$Fe^{3+}/\Sigma Fe$ C2
Standards				
Almandine	7113.0	7122.8	0.00	–
Magnetite	7114.6	7125.5	0.67	–
Hematite	7115.6	7126.2	1.00	–
Garnet #11				
(A') 1	7113.1	7122.9	0.03	0.02
2	7113.1	7122.9	0.03	0.02
3	7113.2	7123.0	0.05	0.04
4	7113.1	7123.2	0.11	0.07
5	7113.1	7123.2	0.11	0.07
6	7113.2	7123.1	0.08	0.06
7	7113.2	7123.2	0.11	0.07
(8)*	(7112.9)	(7123.0)	–	–
9	7113.1	7123.1	0.08	0.06
(10)*	(7113.1)	(7123.5)	–	–
11	7113.1	7123.3	0.14	0.09
12	7113.1	7123.1	0.08	0.06
13	7113.1	7123.2	0.11	0.07
14	7113.1	7123.2	0.11	0.07
15	7113.1	7123.1	0.08	0.06
16	7113.1	7122.9	0.03	0.02
17	7113.1	7123.1	0.08	0.06
18	7113.1	7122.9	0.03	0.02
19	7113.1	7122.9	0.03	0.02
20	7113.1	7123.0	0.05	0.04
21	7113.1	7122.8	0.00	0.00
(B') 22	7113.1	7122.8	0.00	0.00

* Light grey values reported in parenthesis have been rejected because XANES spectra were acquired too close to omphacite inclusions.

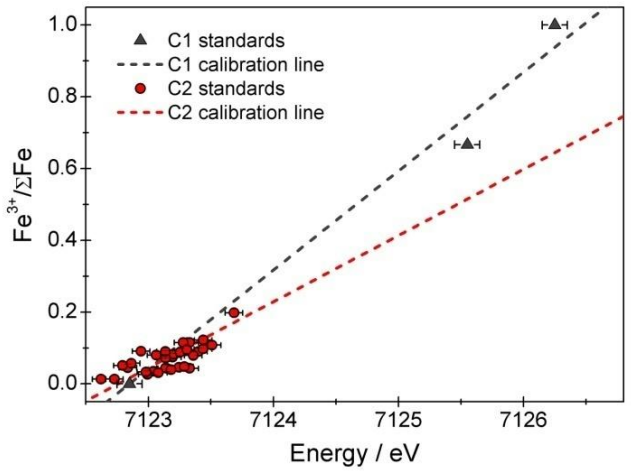

Fig. 5 C1 calibration line obtained using $E_{0.9}$ intensity energy positions for almandine, hematite and magnetite reference minerals (experimental points used to define the calibration line are indicated as dark grey triangles). C2 calibration line obtained using $E_{0.9}$ intensity energy positions from literature data on a complete set of synthetic Fe^{+3}-bearing garnets[22] (experimental points are indicated as red circles). Error bars on $Fe^{3+}/\Sigma Fe$ ratio (± 0.01) are negligible on the scale of this figure.

4.2 Flank Method

We performed combined "flank method" and quantitative elemental analysis profiles on two garnet crystals from the studied sample. The two garnets result significantly zoned[25] as concerning both major elements (Fig. 2b) and $Fe^{3+}/\Sigma Fe$ ratio (Table 2). The physical-chemical principle behind these results is well illustrated in Fig. 6 where a representative emission spectrum of low energy FeL X-rays of Fe^{3+}-bearing garnet is compared with that of Fe^{2+}-bearing garnet. As indicated by the black and grey solid lines, a strong chemical shift occurs between andradite and almandine (Fig. 6a). Also our analysed garnets (Fig. 6b) show an appreciable shift from the core (black spectrum) towards the rim (grey spectrum). This suggests a change in the Fe oxidation state from a Fe^{3+}-richer core to a Fe^{3+}-poorer rim.

The measured Lβ/Lα ratios along the rim-core-rim profile of Grt are reported in Table 2, together with the correspondent calculated $Fe^{3+}/\Sigma Fe$ ratios. It is evident that the $Fe^{3+}/\Sigma Fe$ ratio reaches its maximum in the core ($Fe^{3+}/\Sigma Fe = 0.11$) and progressively decreases towards the rim ($Fe^{3+}/\Sigma Fe = 0.01$).

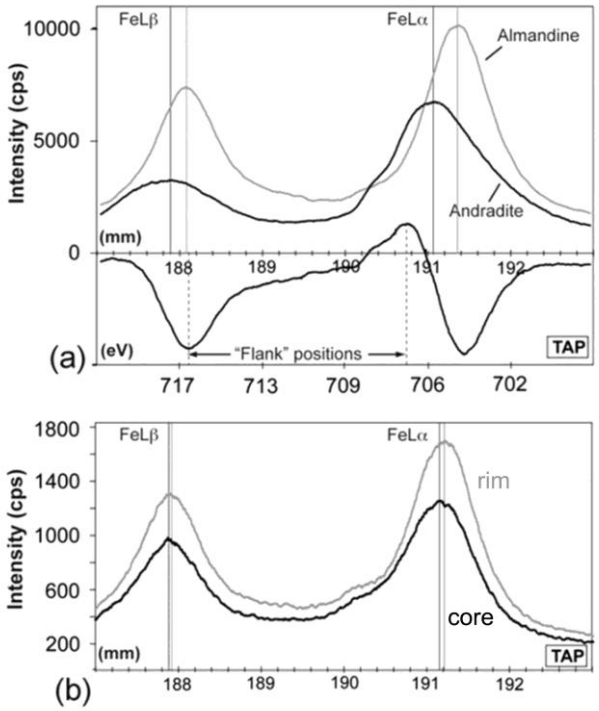

Fig.6 (a) FeL X-ray emission spectra of almandine and andradite, together with the spectrum of the difference between andradite and almandine. The flank method measurement positions (FeLα and FeLβ) correspond to the maxima of the difference spectrum. (b) FeL X-ray emission spectra of the rim of Grt, slightly shifted at higher wavelength positions with respect to its core. In both figures, spectra were collected at 15 kV and 120 nA, with a step size of 5 μm.

Table 2 Lα/Lβ intensity ratios (flank ratios) measured on Grt and corresponding calculated $Fe^{3+}/\Sigma Fe$ ratios.

Sample	Lβ/Lα (cps)	$Fe^{3+}/\Sigma Fe$
Garnet #11		
(A) 1	1.581	0.04
2	1.584	0.04
3	1.599	0.03
4	1.607	0.01
5	1.585	0.03
6	1.567	0.02
7	1.552	0.01
8	1.504	0.02
9	1.456	0.05
10	1.450	0.05
11	1.426	0.05
12	1.374	0.06
13	1.288	0.08
(14)*	1.585	–
15	1.277	0.11
16	1.272	0.10
17	1.316	0.08
18	1.303	0.09
19	1.385	0.03
20	1.385	0.05
(21)	1.374	–
22	1.435	0.04
23	1.410	0.05
24	1.448	0.03
25	1.426	0.07
26	1.598	0.02
27	1.615	0.01
28	1.620	0.01
(B) 29	1.577	0.02

* Light grey values reported in parenthesis have been rejected because flank data were acquired too close to omphacite inclusions.

4.3 Comparison between Micro-XANES and "Flank Method" Results

Fig. 7 reports the $Fe^{3+}/\Sigma Fe$ ratio variation along the two diameters A'-B' and A-B of Grt probed by micro-XANES and "flank method" analysis, respectively. It is evident that both techniques agree in pointing out a progressive decrease in Fe^{3+} content from core to rim. Although the $Fe^{3+}/\Sigma Fe$ trend obtained with the two techniques is comparable, the micro-XANES $Fe^{3+}/\Sigma Fe$ ratios obtained using the C1 calibration are systematically shifted toward higher values with respect to the "flank method" results. This is likely due to the choice of magnetite and hematite as Fe^{3+}-bearing standards, instead of Fe^{3+}-bearing garnets. The agreement between the two techniques is considerably improved considering calibration C2, which is instead obtained using exclusively synthetic Fe^{+3}-bearing garnets. Moreover, as already discussed in Section 4.1, calibration C2 is affected by significantly lower errors with respect to calibration C1.

Since "flank" and micro-XANES acquisitions were performed scanning two different diameters of Grt and the sampling step between two adjacent points was slightly different (13.5 μm for "flank" and 15 μm for micro-XANES), to properly compare $Fe^{3+}/\Sigma Fe$ values obtained with the two methods Grt was divided in a series of compositionally homogeneous regions by processing EMPA compositional maps. As visible in Fig. 8a, the garnet core includes five regions labeled as 1a – 1e, while regions 2a – 2c are assumed to belong to the rim.

Fig. 8b reports the schematic $Fe^{3+}/\Sigma Fe$ zoning of Grt along the sequence of compositional regions previously individuated,

resulting from the "flank method" and the micro-XANES analysis using calibration C2. The absolute $Fe^{3+}/\Sigma Fe$ values obtained with the two techniques are perfectly comparable. XANES values range from a maximum of 0.09 in the garnet core to a minimum of 0.00 in the garnet rim, while "flank" $Fe^{3+}/\Sigma Fe$ ratios vary in the 0.01 – 0.11 interval.

The error bars in Fig. 8b are ± 3% both for the "flank method"[6,29] and for the micro-XANES technique. The errors on the XANES $Fe^{3+}/\Sigma Fe$ ratios are calculated by considering the standard deviation of the fit (σ_f = 0.029) and the uncertainty associated with the adopted monochromator energy step (σ_E = 0.1 eV).

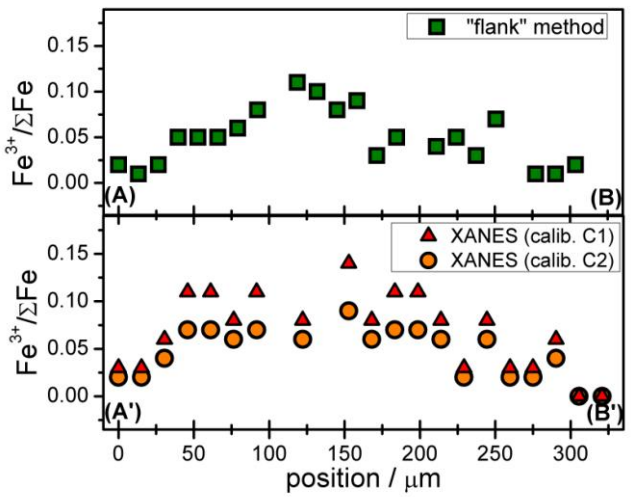

Fig. 7 $Fe^{3+}/\Sigma Fe$ ratio variation along the two diameters A'-B' and A-B of Grt probed by micro-XANES and "flank method" analysis, respectively. For micro-XANES, both the profiles obtained using C1 and C2 calibrations are reported.

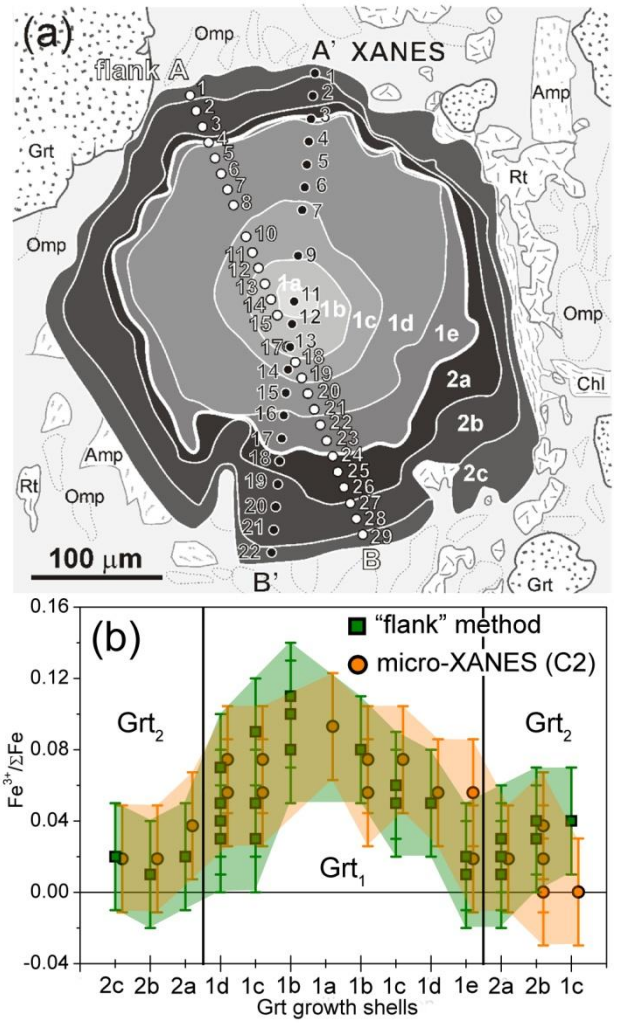

Fig. 8 (a) Schematic sketch of Grt and adjacent minerals within the relevant microstructural site of sample OF2727. Garnet compositional zoning, derived from major elements X-ray maps acquired at SEM-EDS (see Fig. S1 in Supporting Information for further details), consists of eight growth shells (garnet core = 1a – 1e; garnet rim = 2a – 2c). The profiles A-B and A'-B' locate the two sections analysed using the "flank method" and the micro-XANES technique, respectively. The boundary between garnet core and garnet rim is outlined by a thick white line. (b) Compositional profiles for Grt showing the $Fe^{3+}/\Sigma Fe$ as estimated by the micro-XANES using calibration C2 (yellow circles) and "flank method" (green squares) techniques. Micro-XANES and "flank method" data acquired within the same growth shell are compared.

Conclusions

To the best of our knowledge, this study represents the first direct comparison between flank and micro-XANES technique in determining the $Fe^{3+}/\Sigma Fe$ ratios in zoned minerals.

Using micro-XANES technique we were able to successfully estimate $Fe^{3+}/\Sigma Fe$ variations in a single crystal of garnet at a high spatial resolution, obtaining values in very good agreement with $Fe^{3+}/\Sigma Fe$ ratios derived from "flank method". These results thus confirm that micro-XANES spectroscopy is a good method for the determination of the $Fe^{3+}/\Sigma Fe$ ratio in garnet single crystals, because of the good speed of acquisition of XANES spectra and

of the simplicity of sample preparation and data analysis.[22] Furthermore, our results demonstrate that micro-XANES spectroscopy is a valid alternative to the "flank method" for the space-resolved determination of ferric iron contents with micrometric resolution in Fe-bearing minerals. The "flank method" analysis is currently limited to a very small number of mineral phases, namely garnet,[29,63] wustite[64] and amphiboles[65] and, except for garnet, it has been so far applied only on powdered samples. For both the techniques, the difficulty in obtaining reliable quantitative $Fe^{3+}/\Sigma Fe$ estimates on single crystals of non-isotropic minerals is mostly due to the orientation dependence of both the XANES and the "flank method" results. However, once that this difficulty will be overcome, the two techniques will be both very promising for a routinely application on single crystals of Fe-bearing minerals.

Summarizing, we have shown (Fig. 8b) that flank and micro-XANES studies reports results of comparable quality in terms of both spatial resolution and errors associated to the $Fe^{3+}/\Sigma Fe$ ratio determination. This means that for any future works the two techniques can be equivalently applied and the choice should only depend on the accessibility that different groups can have to the two techniques. Note also that, at III generation synchrotron radiation sources, impressive improvements in the X-ray optics recently resulted in remarkable narrowing of the X-ray spot size.[66]

Finally the results of this work, combined with the already estimated *P-T* conditions of garnet growth,[25] provide information on the redox processes occurring, at least locally, during subduction of the oceanic crust, and they are thus relevant for the general comprehension of the metamorphic and geochemical processes occurring in the subduction settings. The decrease of $Fe^{3+}/\Sigma Fe$ from garnet core to garnet rim is related to dehydration-redox equilibria that involve the breakdown of lawsonite and chlorite and the release of H_2O and O_2 (see Supporting Information for further details). This suggests that garnet may play a significant role in the production of oxidizing fluids within the subducting slab, possibly affecting the overlying mantle wedge.

Notes and references

[a] *Dept. of Chemistry, University of Turin, via Giuria 7, I-10125 Torino (Italy); NIS Centre of Excellence and INSTM Centro di Riferimento, via Quarello 11, I-10135, Torino (Italy)*
[b] *Dept. of Earth Sciences, University of Torino, via Valperga Caluso 35, I-10125 Torino (Italy)*
[c] *Dept. of Geological Sciences and Geotechnology, Università degli Studi di Milano-Bicocca, Piazza della Scienza 4, I-20126 Milano (Italy)*
[d] *European Synchrotron Radiation Facility, ID22, 6, rue Jules Horowitz, B.P. 220, F-38043 Grenoble cedex (France)*
[e] *Dept. of Earth Sciences, Università degli Studi di Milano, via Botticelli 23, I-20133 Milano (Italy)*
† *Electronic Supplementary Information (ESI) available: [details of any supplementary information available should be included here]. See DOI: 10.1039/b000000x/*

1 I. J. Parkinson and R. J. Arculus, *Chem. Geol.*, 1999, **160**, 409.
2 B. R. Hacker, G. A. Abers and S. M. Peacock, *J. Geophys. Res.-Solid Earth*, 2003, **108**.
3 A. D. Brandon and D. S. Draper, *Geochim. Cosmochim. Acta*, 1996, **60**, 1739.
4 A. H. Peslier, J. F. Luhr and J. Post, *Earth Planet. Sci. Lett.*, 2002, **201**, 69.
5 N. Malaspina, S. Poli and P. Fumagalli, *J. Petrol.*, 2009, **50**, 1533.
6 N. Malaspina, M. Scambelluri, S. Poli, H. L. M. Van Roermund and F. Langenhorst, *Earth Planet. Sci. Lett.*, 2010, **298**, 417.
7 B. R. Frost and C. Ballhaus, *Geochim. Cosmochim. Acta*, 1998, **62**, 329.
8 M. C. Rowe, A. J. R. Kent and R. L. Nielsen, *J. Petrol.*, 2009, **50**, 61.
9 G. T. R. Droop, *Mineral. Mag.*, 1987, **51**, 431.
10 D. Canil and H. S. C. Oneill, *J. Petrol.*, 1996, **37**, 609.
11 V. N. Sobolev, C. A. McCammon, L. A. Taylor, G. A. Snyder and N. V. Sobolev, *Am. Miner.*, 1999, **84**, 78.
12 A. Proyer, E. Dachs and C. McCammon, *Contrib. Mineral. Petrol.*, 2004, **147**, 305.
13 T. Yokoyama and E. Nakamura, *Geochim. Cosmochim. Acta*, 2002, **66**, 1085.
14 C. A. McCammon, *Hyperfine Interact.*, 1994, **92**, 1235.
15 C. A. McCammon, W. L. Griffin, S. R. Shee and H. S. C. O'Neill, *Contrib. Mineral. Petrol.*, 2001, **141**, 287.
16 H. E. Hofer, G. P. Brey, B. Schulzdobrick and R. Oberhansli, *Eur. J. Mineral.*, 1994, **6**, 407.
17 J. S. Delaney, M. D. Dyar, S. R. Sutton and S. Bajt, *Geology*, 1998, **26**, 139.
18 R. Schmid, M. Wilke, R. Oberhansli, K. Janssens, G. Falkenberg, L. Franz and A. Gaab, *Lithos*, 2003, **70**, 381.
19 M. Munoz, V. De Andrade, O. Vidal, E. Lewin, S. Pascarelli and J. Susini, *Geochem. Geophys. Geosyst.*, 2006, **7**.
20 G. M. Yaxley, A. J. Berry, V. S. Kamenetsky, A. B. Woodland and A. V. Golovin, 2012, **140**, 142.
21 A. J. Berry, L. V. Danyushevsky, H. S. C. O'Neill, M. Newville and S. R. Sutton, *Nature*, 2008, **455**, 960.
22 A. J. Berry, G. M. Yaxley, A. B. Woodland and G. J. Foran, *Chem. Geol.*, 2010, **278**, 31.
23 M. Wilke, F. Farges, P. E. Petit, G. E. Brown and F. Martin, *Am. Miner.*, 2001, **86**, 714.
24 M. D. Dyar, E. W. Lowe, C. V. Guidotti and J. S. Delaney, *Am. Miner.*, 2002, **87**, 514.
25 C. Groppo and D. Castelli, *J. Petrol.*, 2010, **51**, 2489.
26 L. A. J. Garvie and P. R. Buseck, *Nature*, 1998, **396**, 667.
27 P. A. van Aken, B. Liebscher and V. J. Styrsa, *Phys. Chem. Miner.*, 1998, **25**, 323.
28 D. J. Frost and F. Langenhorst, *Earth Planet. Sci. Lett.*, 2002, **199**, 227.
29 H. E. Hoefer and G. P. Brey, *Am. Miner.*, 2007, **92**, 873.
30 S. Creighton, T. Stachel, S. Matveev, H. Hofer, C. McCammon and R. W. Luth, *Contrib. Mineral. Petrol.*, 2009, **157**, 491.
31 F. Farges, M. Munoz, R. Siewert, V. Malavergne, G. E. Brown, H. Behrens, M. Nowak and P. E. Petit, *Geochim. Cosmochim. Acta*, 2001, **65**, 1679.
32 C. Lamberti, C. Prestipino, F. Bonino, L. Capello, S. Bordiga, G. Spoto, A. Zecchina, S. D. Moreno, B. Cremaschi, M. Garilli, A. Marsella, D. Carmello, S. Vidotto and G. Leofanti, *Angew. Chem.-Int. Edit.*, 2002, **41**, 2341.

33 V. Magnien, D. R. Neuville, L. Cormier, J. Roux, J. L. Hazemann, D. de Ligny, S. Pascarelli, I. Vickridge, O. Pinet and P. Richet, *Geochim. Cosmochim. Acta*, 2008, **72**, 2157.

34 M. A. Gomez, L. Becze, R. I. R. Blyth, J. N. Cutler and G. P. Demopoulos, *Geochim. Cosmochim. Acta*, 2010, **74**, 5835.

35 S. Cagno, G. Nuyts, S. Bugani, K. De Vis, O. Schalm, J. Caen, L. Helfen, M. Cotte, P. Reischig and K. Janssens, 2011, **26**, 2442.

36 S. Quartieri, G. Antonioli, P. P. Lottici and G. Artioli, *Mineral. Mag.*, 1993, **57**, 249.

37 G. Artioli, S. Quartieri and A. Deriu, *Can. Mineral.*, 1995, **33**, 67.

38 C. Lamberti, S. Bordiga, F. Bonino, C. Prestipino, G. Berlier, L. Capello, F. D'Acapito, F. Xamena and A. Zecchina, *Phys. Chem. Chem. Phys.*, 2003, **5**, 4502.

39 J. Jernstrom, M. Eriksson, J. Osan, G. Tamborini, S. Torok, R. Simon, G. Falkenberg, A. Alsecz and M. Betti, *J. Anal. At. Spectrom.*, 2004, **19**, 1428.

40 R. Le Toquin, W. Paulus, A. Cousson, C. Prestipino and C. Lamberti, *J. Am. Chem. Soc.*, 2006, **128**, 13161.

41 M. Wilke, O. Hahn, A. B. Woodland and K. Rickers, *J. Anal. At. Spectrom.*, 2009, **24**, 1364.

42 N. B. Muddada, U. Olsbye, L. Caccialupi, F. Cavani, G. Leofanti, D. Gianolio, S. Bordiga and C. Lamberti, *Phys. Chem. Chem. Phys.*, 2010, **12**, 5605.

43 N. B. Muddada, U. Olsbye, G. Leofanti, D. Gianolio, F. Bonino, S. Bordiga, T. Fuglerud, S. Vidotto, A. Marsella and C. Lamberti, *Dalton Trans.*, 2010, **39**, 8437.

44 A. Piovano, G. Agostini, A. I. Frenkel, T. Bertier, C. Prestipino, M. Ceretti, W. Paulus and C. Lamberti, *J. Phys. Chem. C*, 2011, **115**, 1311.

45 S. Bajt, S. R. Sutton and J. S. Delaney, *Geochim. Cosmochim. Acta*, 1994, **58**, 5209.

46 S. Cagliero, A. Piovano, C. Lamberti, M. M. R. Khan, A. Agostino, G. Agostini, D. Gianolio, L. Mino, J. A. Sans, C. Manfredotti and M. Truccato, *J. Synchrotron. Radiat.*, 2009, **16**, 813.

47 L. Mino, A. Agostino, S. Codato and C. Lamberti, *J. Anal. At. Spectrom.*, 2010, **25**, 831.

48 L. Mino, D. Gianolio, G. Agostini, A. Piovano, M. Truccato, A. Agostino, S. Cagliero, G. Martinez-Criado, S. Codato and C. Lamberti, *Adv. Mater.*, 2010, **22**, 2050.

49 L. Mino, D. Gianolio, G. Agostini, A. Piovano, M. Truccato, A. Agostino, S. Cagliero, G. Martinez-Criado, F. d'Acapito, S. Codato and C. Lamberti, *Small*, 2011, **7**, 930.

50 M. Cotte, J. Szlachetko, S. Lahlil, M. Salome, V. A. Sole, I. Biron and J. Susini, 2011, **26**, 1051.

51 S. Lahlil, M. Cotte, I. Biron, J. Szlachetko, N. Menguy and J. Susini, 2011, **26**, 1040.

52 M. Radepont, W. de Nolf, K. Janssens, G. Van der Snickt, Y. Coquinot, L. Klaassen and M. Cotte, 2011, **26**, 959.

53 G. Martinez-Criado, E. Borfecchia, L. Mino and C. Lamberti, *Micro and nano X-ray beams*, in: Characterization of Semiconductor Heterostructures and Nanostructures II; G. Agostini and C. Lamberti, Ed.; Elsevier: Amsterdam, **2012**.

54 C. M. B. Henderson, G. Cressey and S. A. T. Redfern, *Radiat. Phys. Chem.*, 1995, **45**, 459.

55 Y. Mikhlin, Y. Tomashevich, V. Tauson, D. Vyalikh, S. Molodtsov and R. Szargan, *J. Electron Spectrosc. Relat. Phenom.*, 2005, **142**, 83.

56 J. R. Hayes and A. P. Grosvenor, *J. Phys.-Condes. Matter*, 2011, **23**, Art. n. 465502.

57 D. Castelli and B. Lombardo, *Ofioliti*, 2007, **32**, 1.

58 A. Somogyi, R. Tucoulou, G. Martinez-Criado, A. Homs, J. Cauzid, P. Bleuet, S. Bohic and A. Simionovici, *J. Synchrot. Radiat.*, 2005, **12**, 208.

59 R. Tucoulou, G. Martinez-Criado, P. Bleuet, I. Kieffer, P. Cloetens, S. Laboure, T. Martin, C. Guilloud and J. Susini, 2008, **15**, 392.

60 P. Kirkpatrick and A. V. Baez, *J. Opt. Soc. Am.* , 1948, **38**, 766.

61 J. A. Bearden and A. F. Burr, 1967, **39**, 125.

62 B. Ravel and M. Newville, *J. Synchrot. Radiat.*, 2005, **12**, 537.

63 H. E. Hofer, G. P. Brey and R. Oberhansli, *Phys. Chem. Miner.*, 1996, **23**, 241.

64 H. E. Hofer, S. Weinbruch, C. A. McCammon and G. P. Brey, *Eur. J. Mineral.*, 2000, **12**, 63.

65 M. Enders, D. Speer, W. V. Maresch and C. A. McCammon, *Contrib. Mineral. Petrol.*, 2000, **140**, 135.

66 G. Martinez-Criado, R. Tucoulou, P. Cloetens, P. Bleuet, S. Bohic, J. Cauzid, I. Kieffer, E. Kosior, S. Laboure, S. Petitgirard, A. Rack, J. A. Sans, J. Segura-Ruiz, H. Suhonen, J. Susini and J. Villanova, 2012, **19**, 10.